Structure and Activity of Activated Carbon Functionalized with Maleic Anhydride by Diels-Alder Reaction

Lina Mahardiani,[a,b] *Abhijit Shrotri,*[a] *Hirokazu Kobayashi,*[a] *Atsushi Fukuoka*[a]*

[a]Institute for Catalysis, Hokkaido University, Kita 21 Nishi 10, Kita-Ku, Sapporo, Hokkaido 001-0021, Japan. Corresponding author: Atsushi Fukuoka, email: fukuoka@cat.hokudai.ac.jp

[b]Department of Chemistry Education, Faculty of Teacher Training and Education, Sebelas Maret University, Jl. Ir. Sutami 36A, Kentingan - Surakarta, 57126, Central Java, Indonesia

ABSTRACT. Diels-Alder reaction is a useful method for modifying the surface of carbon materials. In this work, we functionalized activated carbon with a large number of carboxyl groups using the Diels-Alder reaction. Polyaromatic structure of activated carbon acted as a diene for addition of maleic anhydride (MA) that acted as a dienophile. Upon hydrolysis of the anhydride group in the adduct, vicinal carboxyl groups were formed. The formation of carboxyl groups by Diels-Alder reaction was proved by FTIR, solid-state ^{13}C NMR, CO and CO_2 evolution from TPD and Boehm titration. Titration results showed that the number of carboxyl groups increased from 0.09 mmol g^{-1} to 3.06 mmol g^{-1}. DFT calculation showed that the concave site of the armchair edge on carbon surface was the most favorable for the Diels-Alder addition.

The formation of exo-adduct was preferred with a reaction energy (ΔE) of -24 kJ mol^{-1}. The synthesized catalyst was tested for acid-catalyzed hydrolysis of cellobiose. The catalyst showed higher activity than a catalyst prepared by oxidation in the presence of air.

Keywords:

Activated Carbon, Diels-Alder Reaction, Acid Catalyst, Hydrolysis of Cellobiose

1. Introduction

Porous carbon materials have found wide application in many areas such as catalysis, adsorption, gas storage and separation [1,2]. The widespread application of carbon materials is a result of their many favorable properties. Carbon materials are thermally and chemically stable making them durable even under harsh condition. Porous carbon materials can have very high surface areas, so that they are ideal for use in catalysis and adsorption [3]. Finally, the easy availability and inexpensive synthesis of activated carbons makes them cost-effective at any scale of operation [4].

In catalysis, activated carbon is extensively used as a support for the preparation of metal catalysts. The role of carbon as a support is to achieve high dispersion of metal. However, carbon material functions more than just a support and it may affect the catalytic activity by assisting with adsorption of chemicals and by interacting with the substrate to activate it [5]. Consequently, carbon materials are used as catalysts for many reactions. The activity of metal-free carbon catalyst is derived from the nature and abundance of the functional groups present on its surface [6]. Covalent functionalization of the carbon surface can introduce acidic and basic functional

groups that act as catalytically active sites [7]. Functionalized carbon materials find application in both liquid phase [8] and gas phase [9] reactions.

Carbon materials containing covalently bonded carboxyl groups are used for acid-catalyzed reactions such as methanol oxidation [10] and hydrolysis of cellulose [11]. The activity of carbon catalyst with carboxyl groups can be improved by incorporation of vicinal dicarboxylic moieties. For example, the synergy of adjacent functional groups can be employed for hydrolysis of β-1,4-glycosidic bonds in cellobiose [12]. Remarkably high frequency factor was observed for the hydrolysis of cellobiose using phthalic acid as a dicarboxylic model catalyst. It is important to note that not only a large number of carboxyl groups but also their position defines the reactivity of carbon materials. However, selective functionalization of carbon materials to incorporate adjacent carboxyl groups is challenging.

Oxidation is the most common method for the introduction of oxygenated functional groups on carbon. Oxidation introduces various kinds of acidic and non-acidic functional groups. The relative density of carboxyl groups increases by using harsh condition for oxidation. Strong oxidizing agents such as nitric acid provide higher density of carboxyl groups [13]. Similarly, when carbon is oxidized in the presence of air, the selectivity of formation of carboxyl groups increases at higher temperature [11]. However, a large number of other functional groups such as hydroxyl, carbonyl, ether and lactone are always present [14]. More importantly, oxidation lacks specific control of the location of functional groups.

One promising approach for selective functionalization of carbon is the Diels-Alder reaction, which involves a [4+2] cycloaddition between a diene and a dienophile to form a stable cyclohexene adduct (Scheme 1) [15]. Diels-Alder reaction is used for covalent functionalization of carbon nanotubes and porous carbon materials to alter the surface features [16–20].

Dienophiles such as tetracyanoethylene and maleic anhydride show high reactivity due to the presence of strong electron withdrawing groups.

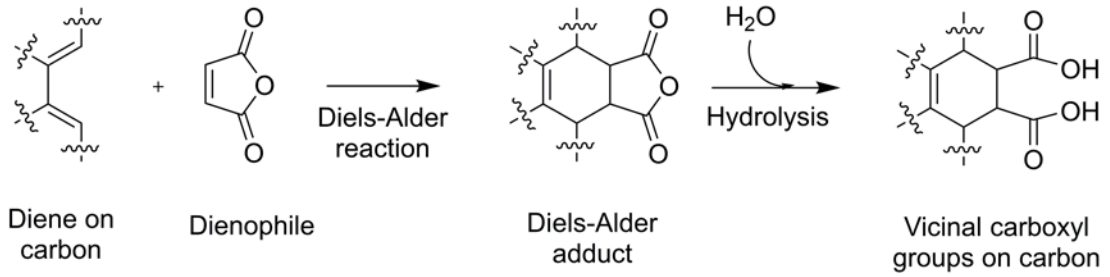

Scheme 1: Strategy for incorporation of vicinal carboxyl groups on carbon surface by Diels-Alder reaction.

The Diels-Alder reaction on activated carbon surface is not completely understood. Activated carbon has a non-uniform structure, and physical properties like curvature in the aromatic plane influence the addition reaction [21]. Materials like fullerene, carbon nanotubes and graphene show different reactivity towards Diels-Alder reaction based on the curvature of their aromatic structure [22]. The polyaromatic plane, arm chair edge and zigzag edge of carbon materials are possible sites for the reaction. In complex carbon materials like activated carbon, it is difficult to determine the favorable site for the Diels-Alder reaction.

Here we report the introduction of vicinal carboxyl groups on activated carbon by Diels-Alder reaction with maleic anhydride. The prepared catalyst was characterized by N_2 adsorption, FTIR, Boehm titration, ^{13}C CP/MAS NMR, TPD and Raman spectroscopy. We also elucidate the plausible position of adduct formation by DFT calculations, and the catalytic activity of the carbons was tested in hydrolysis of cellobiose.

2. Materials and methods

2.1 Chemicals and materials

Activated carbon (named AC) was supplied by Ajinomoto Fine-Techno. Maleic anhydride (>99%), sodium bicarbonate (>99.5%), sodium hydroxide (>97%), toluene (>99.5%), potassium bromide (FTIR grade, crystal block) and standard solutions of 0.05 mol L^{-1} HCl and 0.05 mol L^{-1} NaOH were purchased from Wako Pure Chemical Industries. Cellobiose and ethanol were purchased from Kanto Chemical.

2.2 Catalyst preparation

Activated carbon (AC) was dried in an oven at 120 °C for 2 h. For Diels-Alder reaction, 1.0 g of dried AC and 10.0 g of maleic anhydride were added to a glass tube and purged with Ar for 15 min. Then, the mixture was heated at 120 °C in an oil bath for 7 days under constant stirring using a magnetic stirrer. The mixture was then cooled to room temperature and the slurry was washed with toluene in a Soxhlet extractor. Finally, the obtained carbon was dried in oven at 110 °C for 18 h followed by drying in vacuum for 3 h (named AC-MA). Air-oxidized carbon catalyst was prepared by heating 4 g of dried AC spread with a thickness of 3-5 mm in a furnace at 425 °C for 10 h. The recovered carbon was named AC-Air.

2.3 Characterization

Temperature-programmed desorption (TPD) was performed in a BelCat II from MicrotracBEL. For each run, 50 mg of catalyst was pretreated at 150 °C for 1 h under He flow of 30 mL min^{-1}, followed by raising the temperature from 150 °C to 1000 °C with a ramp rate of 10 °C min^{-1} under He flow. The evolution of CO and CO_2 were determined by the intensities of m/z at 28 and 44, respectively, using a BelMass spectrometer. Calibration for CO and CO_2 was performed after each run.

The acid sites on the surface were characterized by neutralization method described by Boehm [23,24]. NaOH and $NaHCO_3$ were used to neutralize the acid sites followed by back titration to determine the amount of base consumed. For each analysis, 100 mg of catalyst was stirred in 20 mL of 0.05 M $NaHCO_3$ or NaOH solution for 24 h at room temperature. The slurry was filtered and 10 mL of 0.05 M HCl was added to 5 mL of each filtrate. The resulting solution was titrated with 0.05 M NaOH using methyl orange as indicator. The amount of $NaHCO_3$ consumed during neutralization was attributed to the carboxyl groups and the amount of NaOH consumed was attributed to the total number of acid sites.

Fourier transformed infrared spectrum (FTIR) of catalysts was measured using a Perkin Elmer Spectrum 100 S instrument. Before analysis the samples were diluted using KBr (0.1 wt %) and pressed into a pellet. The nitrogen adsorption and desorption isotherms were measured at -196 °C using a Belsorp mini II. Before the adsorption measurements, the samples were outgassed for 3 h under vacuum at 110 °C. The surface area was calculated by the Brunauer–Emmett–Teller (BET) method. Solid state ^{13}C CP/MAS NMR was measured on a Bruker MSL-300 instrument (75.4 MHz, MAS 8 kHz, relaxation delay 1 s). Raman spectra were obtained from Renishaw inVia Reflux spectroscope using 532 nm laser. For each spectrum, eight scans were collected in the 1000-2000 cm^{-1} region.

2.4 Theoretical calculation

The density functional theory (DFT) calculations were performed with the Gaussian 09 programs. Chemical structures and the energies were estimated at the M06-2X/6-31+G(d,p) level of theory [25,26], because the functional predicted the energy of Diels-Alder reactions in good accuracy [27]. Zero-point vibration energies were included in the energy calculation.

2.5 Catalytic activity test

Hydrolysis of cellobiose was conducted in a pressurized Ace glass reactor where cellobiose (40 mg) was mixed with carbon catalyst (6.2 mg) in 5 mL of H_2O for 6 h at 140 °C. Then the mixture was centrifuged to separate the filtrate and solid. Conversion of cellobiose and yield of products was calculated by analyzing the filtrate using a high-performance liquid chromatograph (Prominence, Shimadzu) equipped with a Shodex Sugar SH-1011 column. Yield of unknown products was calculated by subtracting the total yield of known products from the conversion.

3. Results and Discussion

Activated carbon AC was treated with maleic anhydride in solvent-free condition at 120 °C to complete the Diels-Alder reaction. The resulting catalyst showed an increase in mass of 51% because of the incorporation of maleic anhydride on the carbon surface (Table 1). AC-Air prepared by oxidation of activated carbon under air showed a mass loss of 47 % because a part of carbon was lost as CO and CO_2.

Table 1: Summary of chemical and physical properties of carbon materials.

Sample	Change in mass	N_2 adsorption		Boehm titration		TPD		Raman
	%	S_{BET} ($m^2\ g^{-1}$)	Pore volume ($cm^3\ g^{-1}$)	Total acidity (mmol g^{-1})	COOH (mmol g^{-1})	CO (mmol g^{-1})	CO_2 (mmol g^{-1})	I_D/I_G
AC	-	1157	0.61	0.35	0.09	0.88	0.32	0.96
AC-MA	+51	131	0.12	3.11	3.06	1.47	2.66	0.90
AC-MA-3d	+22	405	0.26	1.47	1.41	0.95	1.33	0.90
AC-Air	-47	1057	0.62	2.64	1.00	5.29	1.16	0.91

N_2 adsorption isotherm was measured to analyze physical structures of AC, AC-MA and AC-Air. AC showed an isotherm typical for microporous solid with condensation at $p/p_0 > 0.4$ indicative of interparticle condensation in activated carbon (Figure 1a). The BET surface area of AC was 1157 m^2 g^{-1} (Table 1). NLDFT simulation by using a standard slit model for carbon materials showed that the micropores had a mean size of 0.6 nm [11]. For AC-MA, the adsorption of N_2 was reduced and the BET surface area was 131 m^2 g^{-1}. However, the shape of isotherm was preserved, showing characteristics of a porous material. The reduction in surface area indicated incorporation of functional groups within the micropores of AC causing partial blockage of the narrow pores. By reducing the preparation time for catalyst synthesis to 3 days instead of 7 days we obtained a catalyst with surface area of 405 m^2 g^{-1}. The N_2 adsorption isotherm of AC-Air was identical to that of AC with a slight reduction in surface area to 1057 m^2 g^{-1} (Table 1). Therefore, the microporous structure of carbon was also preserved after air oxidation.

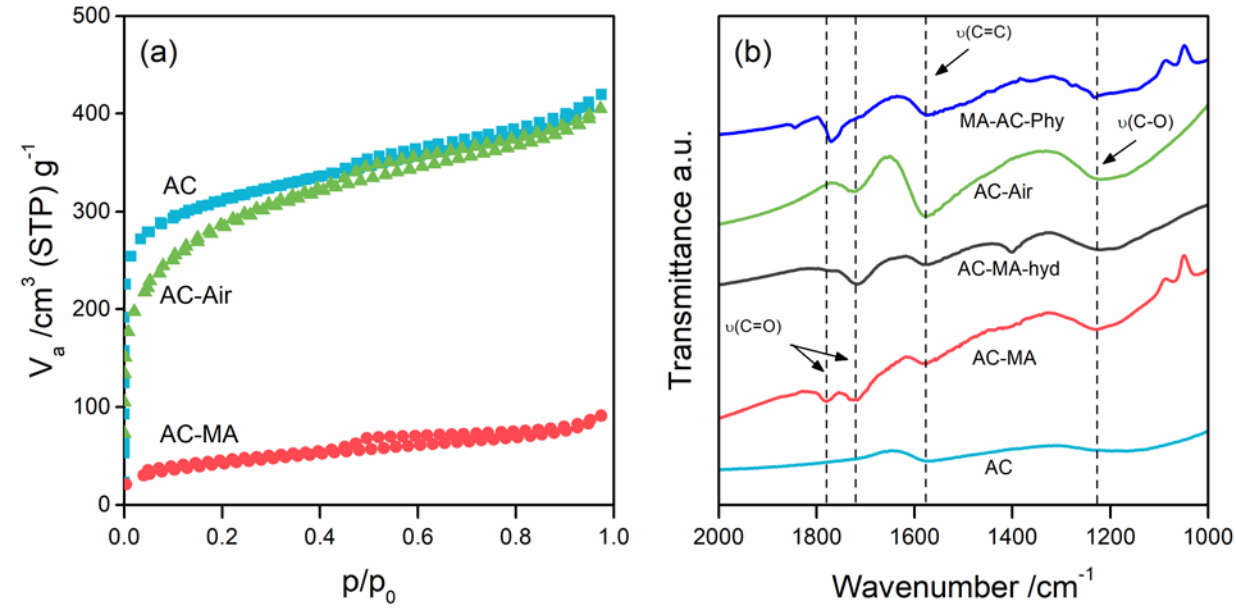

Figure 1: (a) Nitrogen adsorption isotherms of carbon materials. (b) FTIR spectra of AC, AC-MA, AC-MA-hyd (AC-MA after hydrolysis in water at room temperature), AC-Air and MA-AC-Phy (Physical mixture of MA and AC).

FTIR spectra of the carbon materials are shown in Figure 1b. Unreacted AC showed peaks assigned to ν(C=C) in aromatic carbon at 1569 cm^{-1} and overlapping peaks at 1250-1140 cm^{-1} originating from ν(C–O) and other functionalities. After maleic anhydride grafting, two peaks appeared at 1781-1715 cm^{-1} derived from the ν(C=O) of anhydride and carboxyl functional groups [17,20,28,29]. It is evident that part of anhydride groups on the surface of carbon were hydrolyzed to carboxyl groups. The anhydride group is highly reactive and can be hydrolyzed by water present in air to form carboxyl groups. When this sample was hydrolyzed by stirring it in water at room temperature, the ν(C=O) peak from anhydride at 1781 cm^{-1} disappeared, confirming the complete hydrolysis of anhydride to vicinal carboxyl groups. The IR spectrum for the physical mixture of MA and AC showed a single peak for ν(C=O) of the unattached MA centered at 1770 cm^{-1} confirming the absence of free MA species on the carbon surface. The IR spectrum for AC-Air also showed peaks resulting from ν(C=O) of carboxyl groups. Broad peaks of ν(C–O) at 1218 cm^{-1} were observed, indicating incorporation of other functional group such as hydroxyl and ether.

Solid state ^{13}C CP/MAS NMR spectrum of AC showed only one peak assigned to aromatic carbon atoms centered at 125 ppm (Figure 2) [20,30]. Although AC contained small number of oxygenated functional groups, they did not appear in the spectrum due to the low resolution of the CP/MAS NMR analysis. AC-MA showed two additional broad peaks apart from the aromatic carbon. Peaks around 170 ppm were assigned to carbon with $–CO_2R$ from carboxyl and

anhydride groups [20]. Another broad peak at ca. 30 ppm was assigned to sp^3 hybridized carbon in the maleic anhydride adducts [31]. It is notable that the intensity of this peak was high due to cross polarization. Spectrum of AC-Air showed only small peaks centered at 155 ppm and 189 ppm originating from $–CO_2R$ and C–O, respectively.

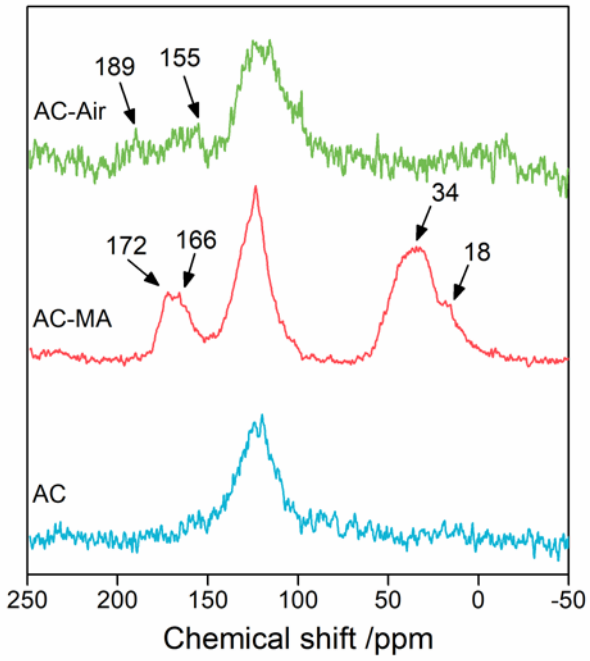

Figure 2: Solid state ^{13}C CP/MAS NMR of carbon materials.

Titration of AC revealed the presence of small number of acidic functional groups (0.35 mmol g^{-1}, Table 1). The total number of COOH in this sample was 0.09 mmol g^{-1}, roughly a fourth of the total acid sites. After incorporation of maleic anhydride, the number of COOH increased to 3.06 mmol g^{-1}. The total number of acid sites in AC-MA was 3.11 mmol g^{-1}, which was similar to that of COOH. This result indicates that only carboxyl groups were incorporated on the carbon surface and no products resulting from degradation of maleic anhydride were present. The AC-MA-3d catalyst showed lower abundance of acidic functional groups (1.41 mmol g^{-1}), suggesting

that 7 d reaction was required to achieve high loading. The titration of AC-Air revealed that the total acidic functional groups was 2.64 mmol g^{-1} including 1.00 mmol g^{-1} of COOH. Therefore, after air oxidation the selectivity of carboxyl groups among all acidic functional groups was 38 %. The remaining 62 % comprised of less acidic sites such as hydroxyl and lactone.

To further characterize the nature of the oxygenated functional groups, we performed TPD [28,32,33] under He flow. The gases evolved during TPD were analyzed using a mass spectrometer. The rates of CO and CO_2 evolution for AC, AC-MA and AC-Air are shown in Figure 3. In accordance with the titration data the evolution of CO_2 (2.66 mmol g^{-1}) and CO (1.47 mmol g^{-1}) from AC-MA showed the presence of high density of carboxyl groups. The decomposition of functional groups in AC-MA started at 190 °C and peaked at 283 °C, which is lower than that of AC-Air. The adducts of Diels-Alder reaction are bonded by single sigma bonds with the surface of carbon materials. Therefore, thermal decomposition of the adducts is easier than that of the carboxyl groups attached to the aromatic carbon. Furthermore, dicarboxylic acids may decompose either by evolution of two CO_2 molecules or by dehydration to produce an anhydride followed by decomposition to produce CO_2 and CO. Therefore, the presence of some amount of CO in TPD of AC-MA is not surprising. Evolution of CO in AC-Air was observed in the temperature range of 420–860 °C. Interestingly, the evolution of CO from AC-Air was very high (5.29 mmol g^{-1}) with the peak centered at 660 °C. It is evident that a large number of non-acidic oxygenated groups such as C=O and C-O-C were also incorporated by air oxidation.

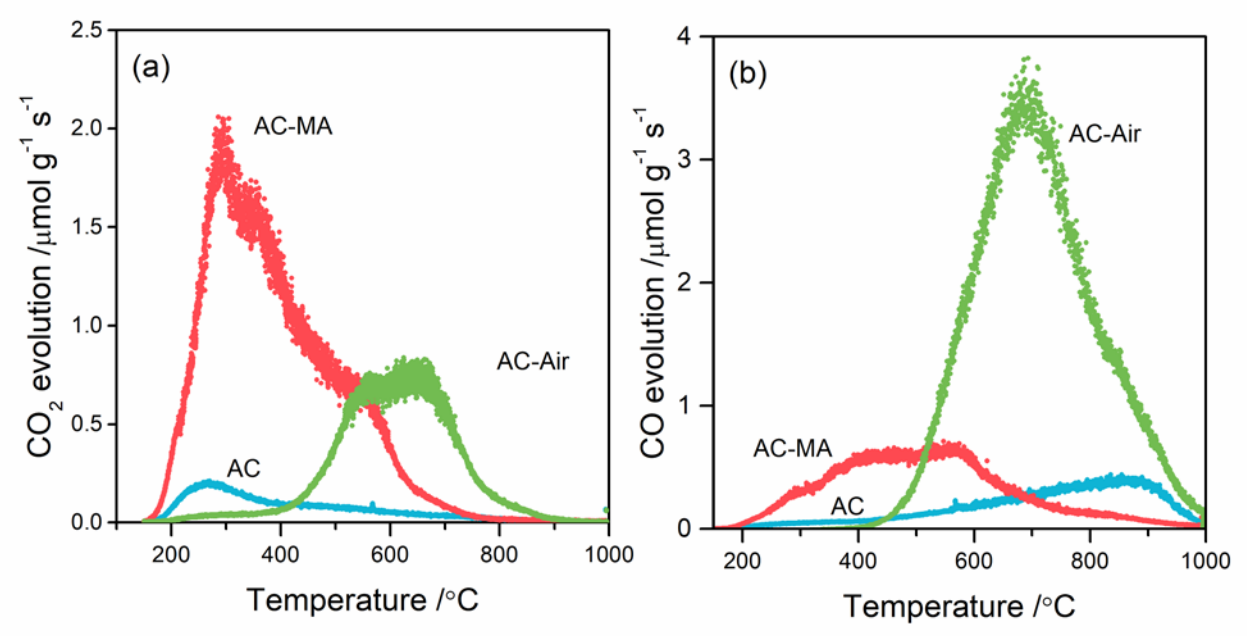

Figure 3: TPD of (a) CO_2 and (b) CO for AC, AC-MA and AC-Air.

Addition of maleic anhydride can occur either on the polyaromatic plane or the edge in carbon materials. The adduct formation on edge would be preferred as the polyaromatic surface probably acts as adsorption site for organic substrates. The preference for the formation of Diels-Alder adduct is based on the curvature in the polyaromatic plane. Curvature introduces sp^3 character on the carbon atoms that favors addition on the surface instead of the edges [21]. Presumably, activated carbon has a disordered structure with curved fragments that lack long range order. Therefore, it is difficult to predict the site for Diels-Alder reaction.

To determine the location of adduct, we performed Raman spectroscopy of the samples. The Raman spectra showed G band (graphitic carbon) arising from in-plane bond stretching of sp^2 carbon pairs at 1592 cm^{-1} for AC (Figure 4). The D band (defect) arising from the presence of defects and functional groups was located at 1344 cm^{-1} [34-36]. The intensity ratio of D band and G band (I_D/I_G) was 0.96 for untreated AC. After MA addition, the I_D/I_G ratio decreased to

0.90, suggesting a slight increase in the graphitic order. This result is in contrast with the functionalization of carbon nanotubes where addition reaction on the cylindrical wall of nanotubes increased the I_D/I_G ratio [37]. Therefore, it is likely that the addition of maleic anhydride occurred at the edge instead of the polyaromatic plane.

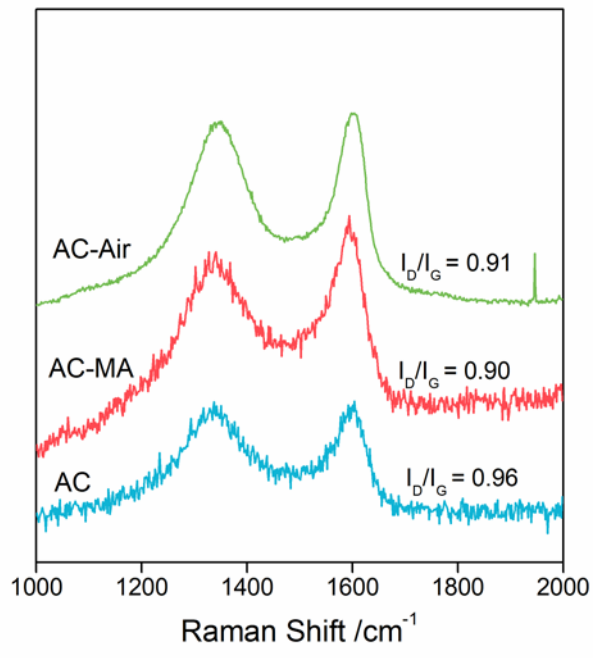

Figure 4: Raman spectra of carbon materials along with the corresponding I_D/I_G ratio.

We also studied the formation of Diels-Alder adduct using DFT calculations. The reaction sites were classified into four types: internal part of surface graphene sheet, concave position in armchair edge, convex position in armchair edge and zigzag edge (Figure 5a-d). First, the Diels-Alder reaction at the internal site (Figure 5a), modelled by coronene, gave a reaction energy including electronic and zero-point vibration (ΔE) of +233 kJ mol^{-1} (Table 2). A large structural distortion due to the formation of sp^3 carbon atoms inside the flat graphene sheet disfavors this reaction. Second, 1,12-benzoperylene was used as a model of concave sites in armchair edges of

carbon materials (Figure 5b). For this compound the formation of exo-type product was energetically favorable (ΔE = –24 kJ mol^{-1}). Endo-type product was less stable than the exo-product due to the steric repulsion commonly found in Diels-Alder reactions (ΔE = –17 kJ mol^{-1}, Figure 5e). We employed a bilayer of 1,12-benzoperylene to include the stacking effect of graphene layers, which resulted in a similar reaction energy for the production of exo-type compound (–30 kJ mol^{-1}). In contrast to concave sites, the calculation for coronene has indicated that a convex site does not undergo the Dies-Alder reaction (+112 kJ mol^{-1}, Figure 5c). For a zigzag edge, the Dies-Alder reaction may not occur as diene structure is only available inside of the graphene sheet (Figure 5d). Instead, we calculated an addition reaction using peri-naphthacenonaphthacene and maleic anhydride, which was unstable (+29 kJ mol^{-1}). Accordingly, the concave position of armchair edge is the most probable site for the Diels-Alder reaction.

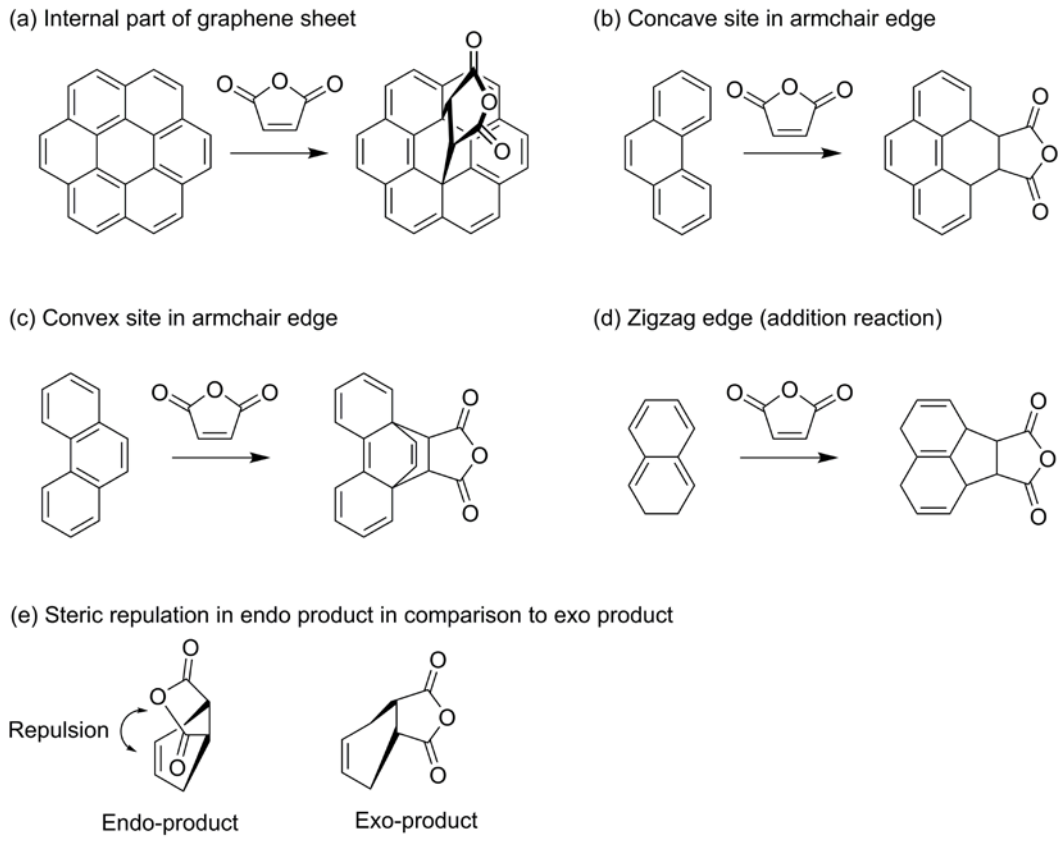

Figure 5: (a-d) Possible sites for Diels-Alder addition of maleic anhydride on model compounds. (e) Steric repulsion in formation of endo-product in comparison to exo-product.

Table 2: Energy of Diels-Alder reaction with maleic anhydride determined by DFT calculations at the M06-2X/6-31+G(d,p) level.

Reaction site	Model substrate[a]	Product conformation	ΔE^a /kJ mol^{-1}
Internal part of graphene sheet	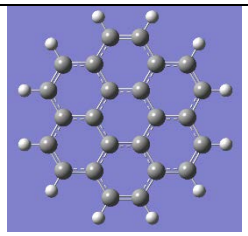 Coronene	–	+233

Concave site of armchair edge	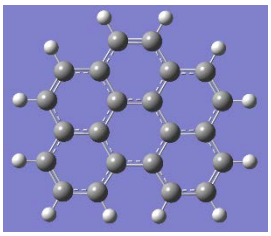 1,12-Benzoperylene	Exo	–24
Concave site of armchair edge	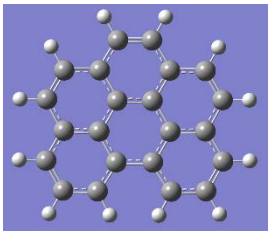 1,12-Benzoperylene	Endo	–17
Concave site of armchair edge	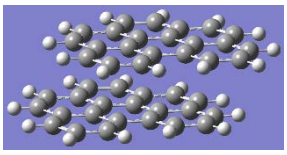 Bilayer of 1,12-benzoperylene	Exo	–30
Convex site of armchair edge	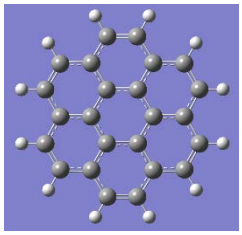 Coronene	Exo	+112
Zigzag edge	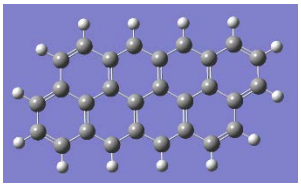 Peri-naphthacenonaphthacene	Exo[b]	+29

[a]Total energy change in the reaction including electronic and zero-point vibration energy. [b]Addition reaction; spin state of the product is triplet.

The catalytic activity of AC-MA was tested for aqueous phase hydrolysis of cellobiose at 140 °C and substrate to catalyst ratio (S/C) of 6.5. In the absence of catalyst cellobiose conversion was 21 % with a glucose yield of 12 % (Table 3). AC and AC-Air showed similar activity with glucose yield of 28 % and 27 %, respectively. In the presence of AC-MA the cellobiose conversion increased to 50 % and glucose yield was 41 %. By-products such as sugar isomers (1.0 %), levoglucosan (0.5 %), 5-HMF (0.4 %) and furfural (0.3 %) were also detected. The high density of carboxyl groups in AC-MA and their vicinal location could be attributed to the increased activity of catalyst for cellobiose hydrolysis. Upon extending the reaction time maximum glucose yield of 75 % was obtained with 94 % conversion of cellobiose. Further increase in glucose yield was not possible due to formation of unknown by-products. These results are comparable to the previous reports for cellulose hydrolysis using oxygenated carbon catalysts. Activated carbon oxidized in the presence of nitric acid showed 94 % conversion of cellobiose with 77 % selectivity for glucose after 24 h reaction at 120 °C and a low S/C = 1 [38]. In another study, graphene oxide showed 79 % cellobiose conversion and 66 % glucose yield after 24 h reaction at 150 °C with an S/C = 6.75 [39]. Therefore, we conclude carbon catalyst containing vicinal functional groups show high activity for cellobiose hydrolysis.

Table 3: Yield of products after hydrolysis of cellobiose in the presence of carbon catalysts[a].

Entry	Catalyst	Time (h)	Conversion (%)	Product Yield (%)				
				Glucose	Isomers[b]	Levoglucosan	5-HMF	Furfural
1	None	6	21	12	0.6	0.2	1.8	0.1
2	AC	6	34	28	0.7	0.2	0.1	0.0

3	AC-Air	6	33	27	1.5	0.3	0.8	0.4
4	AC-MA	6	50	41	1.0	0.5	0.4	0.3
5	AC-MA	12	85	70	3.8	1.3	1.2	0.2
6	AC-MA	16	94	75	4.1	1.4	1.5	0.3
7	AC-MA	24	96	61	3.6	1.4	3.8	0.6

[a]Reaction conditions: Cellobiose 40 mg, catalyst 6.2 mg, H_2O 5 mL, temperature 140 °C.

[b]Combined yield of fructose and mannose.

4. Conclusions

We aimed to introduce a large number of vicinal carboxyl groups on activated carbon by Diels-Alder reaction of maleic anhydride and evaluated its catalytic activity. After 7 days of reaction at 120 °C the catalyst showed incorporation of a large number of carboxyl groups, which was evidenced by titration and TPD experiment. The presence of carboxyl groups was confirmed by FTIR, ^{13}C CP/MAS NMR and other analytical methods. DFT calculations suggested that the concave part of armchair edge was the most favorable site for formation of Diels-Alder adduct in exo conformation. Owing to the high density of carboxyl groups and their vicinal arrangement the catalyst showed higher activity for cellobiose hydrolysis in comparison to catalyst prepared by air-oxidation of activated carbon.

5. Acknowledgement

This work was supported by JST ALCA Grant Number JPMJAL1309, Japan.

6. References

[1] N. Linares, A.M. Silvestre-Albero, E. Serrano, J. Silvestre-Albero, J. García-Martínez, Mesoporous materials for clean energy technologies, Chem. Soc. Rev. 43 (2014) 7681–7717.

[2] M.-M. Titirici, R.J. White, N. Brun, V.L. Budarin, D.S. Su, F. del Monte, J.H. Clark, M.J. MacLachlan, Sustainable carbon materials, Chem. Soc. Rev. 44 (2015) 250–290.

[3] J. Lee, J. Kim, T. Hyeon, Recent Progress in the Synthesis of Porous Carbon Materials, Adv. Mater. 18 (2006) 2073–2094.

[4] E. Auer, A. Freund, J. Pietsch, T. Tacke, Carbons as supports for industrial precious metal catalysts, Appl. Catal. A Gen. 173 (1998) 259–271.

[5] A.E. Aksoylu, M. Madalena, A. Freitas, M.F.R. Pereira, J.L. Figueiredo, The effects of different activated carbon supports and support modifications on the properties of Pt/AC catalysts, Carbon 39 (2001) 175–185.

[6] J.L. Figueiredo, M.F.R. Pereira, The role of surface chemistry in catalysis with carbons, Catal. Today 150 (2010) 2–7.

[7] J.-P. Tessonnier, R.G. Rao, G. Giambastiani, G. Tuci, Covalent Methods for Functional Carbons' Synthesis, in: Metal-free Functionalized Carbons in Catalysis: Synthesis, Characterization and Applications, The Royal Society of Chemistry, (2018) 1–28.

[8] C.E. Chan-Thaw, Metal-free Functionalized Carbon in Liquid Phase Reactions, in: Metal-free Functionalized Carbons in Catalysis: Synthesis, Characterization and Applications, The Royal Society of Chemistry, (2018) 177–195.

[9] X. Liu, A. Cheruvathur, R. Sharpe, Carbon-based Metal-free Catalysts for Dehydrogenation of Hydrocarbons, in: Metal-free Functionalized Carbons in Catalysis: Synthesis, Characterization and Applications, The Royal Society of Chemistry, (2018)

196–227.

[10] Y. Wang, Q. He, J. Guo, H. Wei, K. Ding, H. Lin, S. Bhana, X. Huang, Z. Luo, T.D. Shen, S. Wei, Z. Guo, Carboxyl Multiwalled Carbon-Nanotube-Stabilized Palladium Nanocatalysts toward Improved Methanol Oxidation Reaction, ChemElectroChem 2 (2015) 559–570.

[11] A. Shrotri, H. Kobayashi, A. Fukuoka, Air Oxidation of Activated Carbon to Synthesize a Biomimetic Catalyst for Hydrolysis of Cellulose, ChemSusChem 9 (2016) 1299–1303.

[12] H. Kobayashi, M. Yabushita, J. Hasegawa, A. Fukuoka, Synergy of Vicinal Oxygenated Groups of Catalysts for Hydrolysis of Cellulosic Molecules, J. Phys. Chem. C 119 (2015) 20993–20999.

[13] C. Moreno-Castilla, M. V López-Ramón, F. Carrasco-Marín, Changes in surface chemistry of activated carbons by wet oxidation, Carbon 38 (2000) 1995–2001.

[14] A. Shrotri, H. Kobayashi, H. Kaiki, M. Yabushita, A. Fukuoka, Cellulose hydrolysis using oxidized carbon catalyst in a plug-flow slurry process, Ind. Eng. Chem. Res. 56 (2017) 14471–14478.

[15] M.A. Tasdelen, Diels–Alder “click” reactions: recent applications in polymer and material science, Polym. Chem. 2 (2011) 2133–2145.

[16] D.R. Dreyer, S. Park, C.W. Bielawski, R.S. Ruoff, The chemistry of graphene oxide, Chem. Soc. Rev. 39 (2010) 228–240.

[17] J.-M. Seo, J.-B. Baek, A solvent-free Diels–Alder reaction of graphite into functionalized graphene nanosheets, Chem. Commun. 50 (2014) 14651–14653.

[18] P.P. Brisebois, C. Kuss, S.B. Schougaard, R. Izquierdo, M. Siaj, New Insights into the Diels-Alder Reaction of Graphene Oxide, Chem. Eur. J. 22 (2016) 5849–5852.

[19] F. Severini, L. Formaro, M. Pegoraro, L. Posca, Chemical modification of carbon fiber surfaces, Carbon 40 (2002) 735–741.

[20] R.K.S. Almeida, J.C.P. Melo, C. Airoldi, A new approach for mesoporous carbon organofunctionalization with maleic anhydride, Microporous Mesoporous Mater. 165 (2013) 168–176.

[21] B. Willocq, V. Lemaur, M. El Garah, A. Ciesielski, P. Samori, J.-M. Raquez, P. Dubois, J. Cornil, The role of curvature in Diels-Alder functionalization of carbon-based materials, Chem. Commun. 52 (2016) 7608–7611.

[22] N. Zydziak, B. Yameen, C. Barner-Kowollik, Diels-Alder reactions for carbon material synthesis and surface functionalization, Polym. Chem. 4 (2013) 4072–4086.

[23] H.P. Boehm, Some aspects of the surface chemistry of carbon blacks and other carbons, Carbon 32 (1994) 759–769.

[24] H.P. Boehm, Surface oxides on carbon and their analysis: a critical assessment, Carbon 40 (2002) 145–149.

[25] W.J. Hehre, R. Ditchfield, J.A. Pople, Self-Consistent Molecular Orbital Methods. XII. Further Extensions of Gaussian-Type Basis Sets for Use in Molecular Orbital Studies of Organic Molecules, J. Chem. Phys. 56 (1972) 2257–2261.

[26] Y. Zhao, D.G. Truhlar, The M06 suite of density functionals for main group thermochemistry, thermochemical kinetics, noncovalent interactions, excited states, and transition elements: two new functionals and systematic testing of four M06-class functionals and 12 other function, Theor. Chem. Acc. 120 (2008) 215–241.

[27] S.N. Pieniazek, F.R. Clemente, K.N. Houk, Sources of Error in DFT Computations of C–C Bond Formation Thermochemistries: π→σ Transformations and Error Cancellation

by DFT Methods, Angew. Chem. Int. Ed. 47 (2008) 7746–7749.

[28] J.-H.H. Zhou, Z.-J.J. Sui, J. Zhu, P. Li, D. Chen, Y.-C.C. Dai, W.-K.K. Yuan, Characterization of surface oxygen complexes on carbon nanofibers by TPD, XPS and FT-IR, Carbon 45 (2007) 785–796.

[29] P.E. Fanning, M.A. Vannice, A DRIFTS study of the formation of surface groups on carbon by oxidation, Carbon 31 (1993) 721–730.

[30] S. Stankovich, D.A. Dikin, R.D. Piner, K.A. Kohlhaas, A. Kleinhammes, Y. Jia, Y. Wu, S.B.T. Nguyen, R.S. Ruoff, Synthesis of graphene-based nanosheets via chemical reduction of exfoliated graphite oxide, Carbon 45 (2007) 1558–1565.

[31] M. Dubois, K. Guérin, E. Petit, N. Batisse, A. Hamwi, N. Komatsu, J. Giraudet, P. Pirotte, F. Masin, Solid-State NMR Study of Nanodiamonds Produced by the Detonation Technique, J. Phys. Chem. C 113 (2009) 10371–10378.

[32] S. Haydar, C. Moreno-Castilla, M.A. Ferro-García, F. Carrasco-Marín, J. Rivera-Utrilla, A. Perrard, J.P. Joly, Regularities in the temperature-programmed desorption spectra of $CO_2$and CO from activated carbons, Carbon 38 (2000) 1297–1308.

[33] S. Kundu, Y. Wang, W. Xia, M. Muhler, Thermal Stability and Reducibility of Oxygen-Containing Functional Groups on Multiwalled Carbon Nanotube Surfaces : A Quantitative High-Resolution XPS and TPD / TPR Study Thermal Stability and Reducibility of Oxygen-Containing Functional Groups on Multiwa, J. Phys. Chem. C (2008) 16869–16878.

[34] A. Cuesta, P. Dhamelincourt, J. Laureyns, A. Martínez-Alonso, J.M.D. Tascón, Raman microprobe studies on carbon materials, Carbon 32 (1994) 1523–1532.

[35] S.-K. Sze, N. Siddique, J.J. Sloan, R. Escribano, Raman spectroscopic characterization of

carbonaceous aerosols, Atmos. Environ. 35 (2001) 561–568.

[36] A. Sadezky, H. Muckenhuber, H. Grothe, R. Niessner, U. Pöschl, Raman microspectroscopy of soot and related carbonaceous materials: Spectral analysis and structural information, Carbon 43 (2005) 1731–1742.

[37] P. Singh, S. Campidelli, S. Giordani, D. Bonifazi, A. Bianco, M. Prato, Organic functionalisation and characterisation of single-walled carbon nanotubes, Chem. Soc. Rev. 38 (2009) 2214–2230.

[38] I. Delidovich, R. Palkovits, Impacts of acidity and textural properties of oxidized carbon materials on their catalytic activity for hydrolysis of cellobiose, Microporous Mesoporous Mater. 219 (2016) 317–321.

[39] X. Zhao, J. Wang, C. Chen, Y. Huang, A. Wang, T. Zhang, Graphene oxide for cellulose hydrolysis: how it works as a highly active catalyst?, Chem. Commun. 50 (2014) 3439–3442.